PCCP

Accepted Manuscript




ROYAL SOCIETY OF CHEMISTRY

www.rsc.org/pccp

PCCP

RSCPublishing

ARTICLE

# Role of Oxygen Vacancies in the Surface Evolution of H at $CeO_2$(111): A Charge Modification Effect

Cite this: DOI: 10.1039/x0xx00000x

Xin-Ping Wu[a,b], Xue-Qing Gong[a,b,*] and Guanzhong Lu[b,*]

Received 00th January 2014,
Accepted 00th January 2014

DOI: 10.1039/x0xx00000x

www.rsc.org/

Diffusions and reactions of H at stoichiometric and reduced $CeO_2$(111) surfaces have been studied by using density functional theory calculations corrected by on-site Coulomb interactions (DFT+U). Oxygen vacancies on the surface are determined to be able to significantly affect the behavior of H by modifying the charge of surface lattice O through the occurrence of $Ce^{3+}$. It has been found that, at the reduced $CeO_2$(111) surface, the adsorption strength of H as well as the H coupling barrier can be dramatically reduced compared to those at the stoichiometric surface, while $H_2O$ formation barrier is not significantly affected. Moreover, the diffusion of H at the reduced surface or into the bulk can occur more readily than that at stoichiometric $CeO_2$(111).

## 1. Introduction

Ceria (cerium dioxide, $CeO_2$) is considered as a promising rare earth catalyst for solar water splitting and $H_2$ production.[1-3] It is also used in numerous other applications, such as the anode of solid oxide fuel cells (SOFCs)[4-7], and supported catalysts like ceria supported vanadium oxides ($VO_x/CeO_2$), which have been shown to be highly active and selective for oxidative dehydrogenation (ODH) reactions[8-12]. For these catalytic processes promoted by different $CeO_2$-based materials, H is a key species on the surfaces. Thus the H-$CeO_2$ interaction is of particular importance and has been widely studied. For surface reactions of H, first-principles studies by Chen et al.[13] provided potential energy profiles at stoichiometric $CeO_2$(111) and (110). Moreover, studies by Bernal et al.[14] suggested that H-$CeO_2$ interaction is only a surface process, while others[15-18] proposed the existence of H infiltration at $CeO_2$, and therefore bulk diffusion of H is also important.

Though many studies[13-18] aiming at understanding the H-ceria interaction have been reported, comprehensive theoretical simulations involving wide range of possible processes are still very rare. For this reason, in this paper, by using density functional theory calculations corrected by on-site Coulomb interactions (DFT+U), we extensively investigated the surface processes of H, including H diffusion, H coupling to generate $H_2$ and $H_2O$ formation accompanied by the formation of a single oxygen vacancy ($O_v$), as well as the bulk diffusion of H (see Fig. S1) at the most stable (111) surface[19,20] of $CeO_2$ to elaborate these competitive H-related processes. It also needs to be mentioned that remarkable catalytic activities of ceria in reactions are widely believed to be related to the existence of oxygen vacancies[21]. Recently, experimental studies[22] also showed that oxygen vacancies play a pivotal role in the reactivity of hydroxyls at $CeO_2$(111) thin films. However, such important effects of oxygen vacancies on H processes at $CeO_2$ surfaces were rarely measured in previous theoretical studies[13,18]. Therefore, in the current work, different reduced surface structures containing single or multiple oxygen vacancies were also considered in an effort to make comparisons with the stoichiometric $CeO_2$(111) surface. It can be also expected that the results obtained at $CeO_2$(111) can be also helpful to understanding similar processes at other facets including $CeO_2$(110) and (100).

Specifically, we found that at stoichiometric $CeO_2$(111), H coupling is more difficult to occur than $H_2O$ formation, and surface diffusion of H can be accelerated with the help of sub-surface oxygen though the overall barriers are still rather high. In addition, the diffusion of H into the bulk is an endothermic process and largely inhibited by the first step of OH bond rotation to point the H toward a sub-surface O. Interestingly, after oxygen vacancies were included in the calculations, it has been found that they can reduce the adsorption strength of H and then influence the diffusion and reaction behavior of H. In general, H coupling, surface diffusion and bulk diffusion are all promoted by at reduced surface, while $H_2O$ formation seems to be much less affected by oxygen vacancies. As a result, H diffusion can occur more readily at reduced $CeO_2$ and $H_2$ generation also becomes competitive with $H_2O$ formation.

## 2. Computational details

Spin-polarized DFT+U calculations were carried out with the GGA-PW91 functional by using the Vienna ab initio Simulation Package (VASP).[23,24] The project-augmented wave method (PAW)[25] was used to describe the electron-core interaction with Ce (5s, 5p, 6s, 5d, 4f), O (2s, 2p) and H (1s) electrons being treated as valence electrons. The on-site Coulomb interaction correction is necessary for the proper description of the localized 4f electron and related electronic and geometric properties of ceria.[26-28] As suggested by Nolan and coworkers,[27,28] the U value was set to 5.0 eV. Wave functions were expanded in plane waves with a kinetic energy cutoff of 400 eV. The calculated lattice parameter of bulk ceria using DFT+U method (5.436 Å) is in good agreement with the experimental value (5.411 Å).[29]

The $CeO_2(111)$ surface was modeled by a 12-atomic-layer slab which represents p(3×3) lateral cells with the bottom three layers being fixed to the bulk parameters, while other layers were allowed to fully relax. To avoid interactions between slabs, all slabs were separated by a vacuum gap greater than 10 Å. All the calculations were converged until the Hellman-Feynman forces on each ion were less than 0.02 eV/Å. The Brillouin-zone integration was performed using a 2×2×1 Monkhorst-Pack grid for each surface.

The nudged elastic band (NEB) method with the climbing-image (CI) modification is an efficient method for finding the minimum energy path (MEP) connecting the given initial and final states.[30-33] In this work, all transition states were located by using the climbing-image nudged elastic band (CI-NEB) method to converge rigorously on the saddle point.

The adsorption energy of H ($E_{ad}(H)$) was calculated as follows:

$$E_{ad}(H) = E_{CeO_x} + \frac{1}{2}E_{H_2} - E_{H/CeO_x},$$

where $E_{CeO_x}$, $E_{H_2}$, and $E_{H/CeO_x}$ represent the DFT total energy of stoichiometric/reduced $CeO_2(111)$, gas-phase hydrogen molecule and H adsorbed stoichiometric/reduced $CeO_2(111)$, respectively.

## 3. Results and discussion

### 3.1 Model construction

In this work, we calculated the H related processes at both stoichiometric and reduced $CeO_2(111)$. For the reduced surfaces, we first considered the $CeO_2(111)$ with one O vacancy. We found that the surface with a sub-surface O vacancy (see Fig. 1) with the two electrons being localized at its second nearest neighbor Ce cations gives the smallest O vacancy formation energy (Table S1 and Fig. S2), which is consistent with other theoretical studies[34,35]. For clarity, we call the surface model with such a sub-surface O vacancy 1OV. To construct a heavily reduced surface, various surface structures containing three surface O vacancies were also calculated. Considering that a surface with three O vacancies has six excess electrons, we expected that it would be difficult to verify the most stable electronic structure. Therefore, we did not intend to search all the possible electronic configurations of all the various structures with three O vacancies. Nevertheless, we found that for the three most stable structures with three neighboring O vacancies, they all contain three neighboring sub-surface O vacancies (Table S2 and Fig. S3). Therefore, in order to study the structural and electronic effects of O vacancies at heavily reduced $CeO_2$, the $CeO_2(111)$ surface with three sub-surface O vacancies ordered in a triangle (see Fig. 1) was taken as the model structure (3OV).

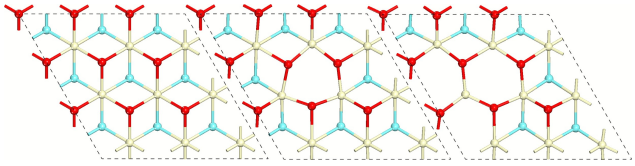

**Fig. 1** Calculated structures (top view of top tri-layer) of stoichiometric $CeO_2(111)$ (left), 1OV (middle) and 3OV (right). Top and sub-surface oxygen atoms are in red and cyan, respectively. Cerium atoms are in ivory. This notation is used throughout the paper.

### 3.2 Adsorption of H

All the processes of surface H are expected to be affected by its adsorption strength. By using the stoichiometric and two reduced surface structures (1OV and 3OV), we first systematically calculated the H adsorption. The optimized adsorption structures clearly showed that the H atom prefers to adsorb directly at the surface O (see Fig. 2), which was also proposed by Vicario et al.[36] Charge analyses further indicated that the electron originated from adsorbed H atom transfers to the surface and at the same time a neighboring Ce cation is reduced from $Ce^{4+}$ to $Ce^{3+}$, which now holds the localized electron (see Fig. S4). In addition, the calculated $E_{ad}(H)$ (1.23 eV at stoichiometric $CeO_2(111)$, 0.98 eV at 1OV and 0.87 eV at 3OV) shows that the H adsorption energy decreases with increasing concentration of O vacancy, i. e. surface with higher concentration of O vacancy gives rise to weaker adsorption strength of H.

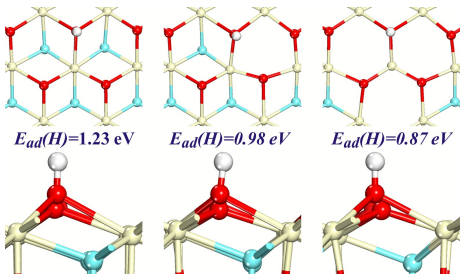


**Fig. 2** Calculated structures (top view: top, side view: bottom) of H adsorption at stoichiometric $CeO_2(111)$ (left), 1OV (middle) and 3OV (right). H atoms are in white. $Ce^{3+}$ distributions before and after H adsorption are shown in Fig. S4. Bader charges (before and after H adsorption) of the three Ce atoms which bond with hydroxyl at three surfaces are listed in Table S3.

### 3.3 H coupling and $H_2O$ formation

Many catalytic reactions like oxidative dehydrogenation at ceria-based catalysts involve H elimination. Surface H can be removed through two possible ways, i.e. (i) $H_2$ formation through H coupling ($H^*+H^* \rightarrow H_2$) and (ii) $H_2O$ formation ($H^*+OH^* \rightarrow H_2O+O_v$). In the current work, these processes were systematically calculated at stoichiometric $CeO_2(111)$ and surfaces with different degrees of reduction (1OV and 3OV). It is clear from Fig. 3 that, when the surface adsorption state of two H ($2H^*$) is taken as the reference, the H coupling barrier at stoichiometric $CeO_2(111)$ (3.51 eV) is significant larger than those at reduced $CeO_2(111)$ (2.93 eV at 1OV, 2.08 eV at 3OV), and higher concentration of O vacancy can give lower barrier. Interestingly, different from H coupling, the $H_2O$ formation starting from the $2H^*$ state, which can be also taken as the reverse process of water dissociation, gives nearly identical barriers of ~1.5 eV at the stoichiometric and the two reduced $CeO_2(111)$ surfaces.

Besides the reaction kinetics, it is also intriguing that O vacancies can have quite remarkable influence on the thermodynamics of surface reactions of H. As one can see from Fig. 3, at stoichiometric $CeO_2(111)$, formation of gas-phase $H_2O$ was calculated to be favored over $H_2$. However, our calculations of the reduced surfaces then showed that the occurrence of one O vacancy can already significantly modify their relative stabilities, and heavily reduced surface like 3OV can even reverse the relative stabilities of the final states with $H_2$ and $H_2O$ formation, though the barrier for the former process is still higher. This is due to the combined effect of

reduced H adsorption energy and increased O vacancy formation energy. Therefore, one may expect that surface adsorbed H at more heavily reduced $CeO_2$ may prefer $H_2$ formation to $H_2O$, which is largely consistent with the experimental results[22]. This may also explain why water splitting can occur at heavily reduced ceria and give rise to $H_2$ under elevated temperatures.[1-3]

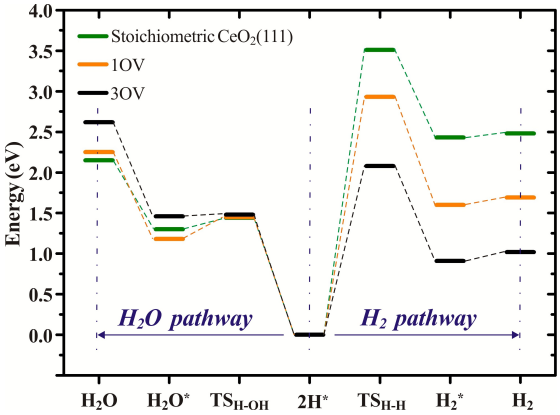


**Fig. 3** Calculated energy profiles for the reactions of two surface adsorbed H to form $H_2$ and $H_2O$ at different $CeO_2$ surfaces with all energies are relative to surface with 2H ($2H^*$). $H_2O$ ($H_2$) is the state with gas-phase $H_2O$ ($H_2$) and $CeO_2$(111). $H_2O^*$ ($H_2^*$) is the $H_2O$ ($H_2$) adsorption state. $TS_{H\text{-}OH}$ ($TS_{H\text{-}H}$) is the transition state to generate $H_2O^*$ ($H_2^*$). Corresponding structures of these key states are illustrated in Fig. S5. Energy barriers are also listed in Table S4.

### 3.4 Surface diffusion of H

Besides surface reactions, adsorbed H may also diffuse on the surfaces. At $CeO_2$(111), two neighboring top-surface O have a distance of ~3.8 Å, while it is ~2.7 Å for that between neighboring top- and sub-surface O. Accordingly, we calculated two different surface diffusion routes at stoichiometric $CeO_2$(111) (see Fig. 4), i.e. (i) direct surface diffusion of H among top-surface O only, and (ii) multi-step surface diffusion involving H transfer between neighboring top- and sub-surface O (Fig. 4). Specifically, since the top-surface OH points the H toward the vacuum, the route (ii) may further involve several elementary steps (see Scheme 1): *1*. Top-surface OH rotates to point the H toward a sub-surface O; *2*. H transfers from top- to sub-surface O; *3*. Sub-surface OH rotates to point H to a top-surface O; *4*. H transfers from sub- to top-surface O; and *5*. Newly formed top-surface OH rotates to point H to the vacuum again. According to our calculation results, route (i) has a very high barrier of 3.49 eV, largely because that the surface structure needs to completely break the O-H bond to reach the transition state ($TS_{DSD}$ in Fig. 4). By contrast, in route (ii), with the help of the sub-surface O, it does not need to completely break the O-H bond of surface hydroxyl group when the H moves to nearby lattice O, making it a better diffusion pathway. Even though, it is still a difficult process as it involves an effective barrier of ~1.5 eV and several unstable intermediate states (see Fig. 4).

From the calculated energy profile of route (ii) at the stoichiometric surface (see Fig. 4), one may also find that the first step that the hydroxyl group rotates to point the H toward the sub-surface O (barrier: 1.15 eV) is the most difficult step. Therefore, at reduced $CeO_2$(111), we only searched the barrier of this first step and found that barriers can be significantly reduced (1.07 eV at 1OV, 0.84 eV at 3OV). It can be expected that further increasing the degree of surface reduction may also facilitate surface H diffusion through such multi-step pathway, unless most of sub-surface O are removed.

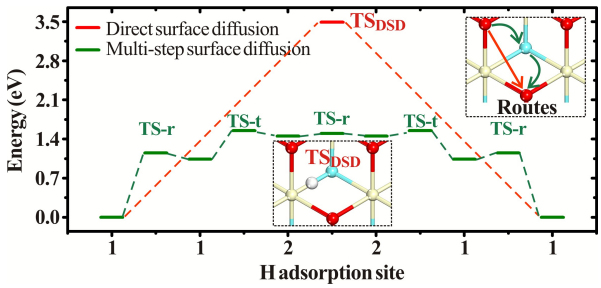


**Fig. 4** Calculated energy profiles for two surface diffusion routes of H at stoichiometric $CeO_2$(111). Numbers at x-axis represent the O layer that the H adsorbs at, e.g. *1* represents the O of (top-surface) 1st O layer. Calculated structures of stable states along the multi-step surface diffusion are shown in Fig. S6. $TS_{DSD}$ is the transition state of the direct surface diffusion (in red). TS-r and TS-t are the corresponding rotation and transfer transition states, respectively, in the multi-step diffusion (in green). Energy barriers are listed in Table S5.

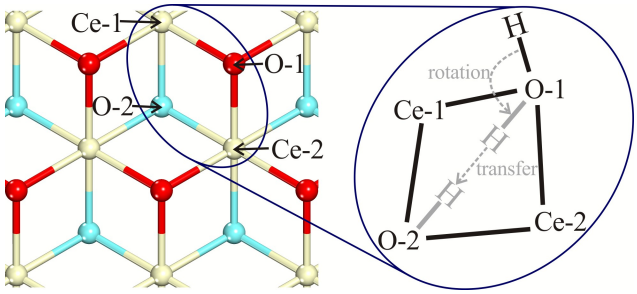


**Scheme 1** A two-step H diffusion mechanism at $CeO_2$(111) (top-view): (i) OH rotation and (ii) H transfer.

### 3.5 Bulk diffusion of H

In this work, H infiltration was also considered as a competitive process with respect to its reactions and diffusions at $CeO_2$ surfaces. We have carefully calculated the H diffusion from the top-surface O to the 5th layer O in our slab model (see Fig. S1). As H diffuses between neighboring O layers in the infiltration process, the two-step H diffusion mechanism illustrated in Scheme 1 is also applicable. In Fig. 5, we illustrate the calculated energy profile of such diffusion process of H at stoichiometric $CeO_2$(111). It is clear to see that this process is endothermic and the most difficult step is the first step of OH rotation (barrier: 1.15 eV), which is actually the same as that in H surface diffusion along route (ii). However, once the H enters the lattice, the subsequent diffusion steps appear to be easy with relatively low barriers. It also needs to be mentioned that the bulk adsorption state of H is much less stable than its surface adsorption state, and the diffusion barriers of the process for it to go back to the surface is rather small (< 0.3 eV, Fig. 5). Therefore, H infiltration can be still largely inhibited.

For H infiltrations at 1OV and 3OV (see Fig. 5), we only calculated the transition states of their first step (the most difficult step). It is again same as the case of surface H diffusion through route (ii) that the barrier for H diffusion to the bulk can be also reduced when oxygen vacancies occur at $CeO_2$(111) (1.07 eV at 1OV, 0.84 eV at 3OV). In addition, the

optimized structures of H adsorption at the lattice O along the diffusion pathway (note: the 3OV structure does not have the second O layer adsorption states due to missing of the corresponding sub-surface O) and lattice O deep into the bulk (calculated with a 18-atomic-layer $CeO_2$(111) slab (17.68 Å thick)) were also determined. The calculated stabilities of these adsorption states follow the trend that more deeply reduced surfaces give more stable adsorption states of H. In particular, an adsorption state of H at the third O layer of 3OV (IM) is rather stable (only 0.22 eV less stable than its surface adsorption state). This is obviously due to the fact that a large empty space was created as the result of the missing of three sub-surface O atoms, which can significantly reduce the unfavorable interaction between the internal hydroxyl and nearby lattice O. However, since such structure is limited within the near sub-surface area, it may hardly facilitate the bulk diffusion of H. But it indeed suggests that if bulk oxygen defects also exist, they can definitely help H bulk adsorption. In general, we can still conclude that the reduced $CeO_2$ would favor H infiltration.

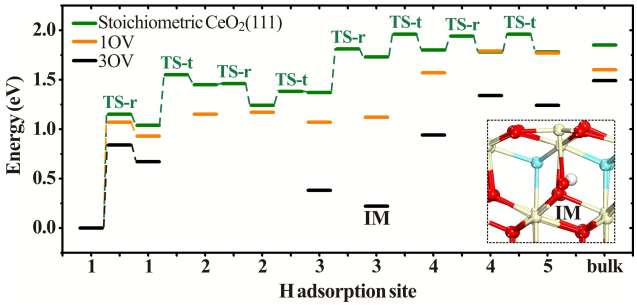


**Fig. 5** Energy profiles for bulk diffusion of H. At 1OV and 3OV, only the barrier of the first rotation step is presented. Numbers at x-axis represent the O layer that the H adsorbs at. TS-r and TS-t are transition states of rotation and transfer processes, respectively. IM is the optimized structure of H adsorbed at the third O layer of 3OV surface slab. Energy barriers are also listed in Table S5.

### 3.6 O-H bond strength and Charge analyses

All the possible H related processes studied in this work involve O-H bond breaking. Therefore to understand the O-H bond strength seems to be important to obtaining deep insight into these processes. In order to conduct a quantitative measurement of such bond strength, we may intuitively decompose the adsorption of H into two procedures: (i) structural deformation of the clean surface to evolve to its corresponding conformation in the adsorption structure with energy cost of $E_d$, and (ii) H binding with deformed surface O with energy gain of $E_b$. Accordingly, the calculated adsorption energy can be divided into two parts: $E_{ad}(H) = -E_d + E_b$ (see Supporting Information for details), and the $E_b$ values calculated in this way are listed in Table 1. It can be easily seen from Table 1 that higher concentration of O vacancy can give rise to lower $E_b$, which indicates a weaker O-H bond.

Moreover, we also performed Bader charge analyses[37-39] (see Table 1) on the hydroxyl O atoms to better understand their activities for H adsorption from an electronic point of view. Before H adsorption, with the increase of surface reduction degree, the calculated Bader charges of top-surface O beside vacancies also increase. This could be due to the fact that localized 4f electrons at reduced $Ce^{3+}$ would significantly affect the electron distributions within its covalent bond with top-surface O and push more covalent electrons toward O. In addition, more $Ce^{3+}$ occurs at 3OV than those at 1OV (see Fig. S4), which leads to a more significant charge modification effect on the O bonding with these $Ce^{3+}$. Accordingly, increased Bader charges can be determined at such top-surface O at 3OV, and they also give rise to weaker OH bonds (Table 1). After H adsorption, the amount of charge on such top-surface O further increases to reduce the total energy of the whole system by enhancing the electrostatic attraction between $O^{\delta-}$ and $H^{\delta+}$. This is consistent with the calculated adsorption structures (see Fig. 2) that the O of the hydroxyl group raises high above other surface lattice O as more charges fill in such O. In addition, one can see from Table 1 that the charges of hydroxyl O atoms (after H adsorption) at three different surfaces are nearly constant, indicating that the original excess charge of surface O at reduced surfaces would then reduce their capability of receiving electrons from adsorbing H. This is consistent with the calculated charge differences of such O before and after H adsorption, which are also listed in Table 1. It should be noted that although the calculated charge values of hydroxyl O atoms (after H adsorption) at these surfaces are very close to each other, the charge distribution of these O atoms are different. At reduced surfaces, more charges distribute at the covalent bond with nearby $Ce^{3+}$, and therefore less charge can be located in the O-H bond, which leads to their different O-H bond strength.

Therefore, we can generally conclude that if the hydroxyl O atom has less charge before H adsorption, more extra charge can be received by such O to fill in the O-H bond and then enhance its bond strength. Such electronic effect can be also reflected in the charge density difference contours of H adsorption (see Fig. 6), which clearly show that less charge transfers to the O-H bond region at reduced surfaces. In other words, these results suggest that existence of O vacancies modifies the charge of neighboring surface O through the occurrence of $Ce^{3+}$, and weakens their O-H bonds after H adsorption. It also needs to be mentioned that for H adsorbed at those top-surface O that do not directly bond with $Ce^{3+}$ at reduced surfaces, the adsorption energy is similar to that at stoichiometric $CeO_2$(111). In fact, we even determined that there is a linear relationship between Bader charge (before H adsorption) of surface O atom and $E_b$, and between $E_b$ and H coupling barrier as well (see Fig. 7). Therefore, our model suggests that the amount of charge of O before H adsorption is rather important as it can simply reflect the O-H bond strength after H adsorption. It is then directly related to the H coupling barrier, and can help estimate the relative difficulty of H surface and bulk diffusions. In conclusion, it can be expected that reactions mainly involving O-H bond breaking such as H coupling can more readily occur at reduced $CeO_2$(111) than at stoichiometric one. At the same time, it also suggests that the surface hydroxyls under reduced conditions are relative unstable, which makes surface and bulk diffusion of H easier as well.

**Table 1** Calculated O-H bond energies ($E_b$) and Bader charges ($e$) of the surface O to which the H binds at stoichiometric and two reduced $CeO_2$(111) (1OV and 3OV).

| | $E_b$ (eV) | Bader charge of the hydroxyl O atom (e) | | |
|---|---|---|---|---|
| | | Before H adsorption | After H adsorption | Charge difference |
| Stoichiometric $CeO_2$(111) | 2.37 | 7.18 | 7.73 | 0.55 |
| 1OV | 2.15 | 7.23 | 7.74 | 0.51 |
| 3OV | 1.86 | 7.29 | 7.74 | 0.45 |

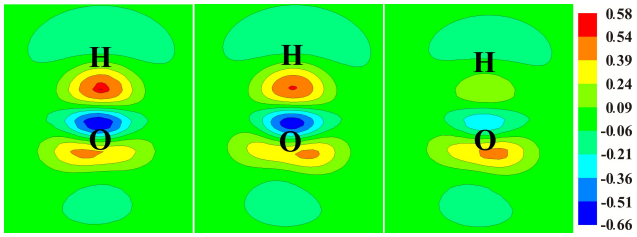


**Fig. 6** Calculated charge density difference contours of H adsorption at stoichiometric $CeO_2(111)$ (left), 1OV (middle) and (c) 3OV (right).

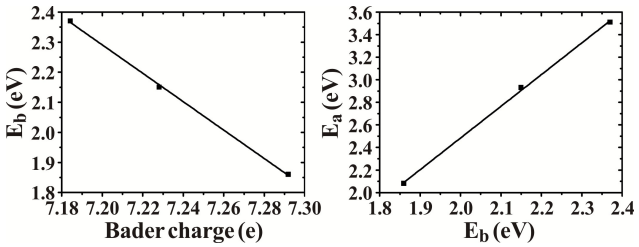


**Fig. 7** Correlations between calculated Bader charges (before H adsorption) of hydroxyl O atoms and $E_b$ (left), and $E_b$ and H coupling barrier ($E_a$) (right).

For $H_2O$ formation, one can see from Fig. S4 that no O-H bond is completely broken in the corresponding transition states ($TS_{H\text{-}OH}$) and it is the OH group that moves to bind with the other adsorbed H. Therefore, the O-H bond strength may no longer significantly affect surface reactivity for water formation. This may be the reason why the $H_2O$ formation barriers are nearly constant at stoichiometric and reduced surfaces.

Herein, our first-principles calculations show that O vacancies can weaken the adsorption strength of H and then promote specific reactions of H at $CeO_2(111)$ through charge modification effects. In particular, we are able to reveal that to reduce the charges of surface O would increase the adsorption strength of H. These findings can be important to understanding hydrogenation and dehydrogenation reactions, and probably also applicable to supported and doped metal-oxide systems in which surface charge distributions are modified as well.

## 4. Conclusions

In this work, by conducting systematic DFT+U calculations and electronic/structural analyses, we have studied the chemical processes of H adsorbed at stoichiometric and various reduced $CeO_2(111)$. At stoichiometric $CeO_2(111)$, the reaction pathway for $H_2O$ formation has lower barrier and more favorable final state compared to those for $H_2$ formation. Therefore, adsorbed H tend to leave the surface through $H_2O$ desorption. In addition, surface diffusion of H at $CeO_2(111)$ with the help of sub-surface oxygen is easier than the direct hoping which involves O-H bond breaking. Nevertheless, the surface diffusion is still very difficult due to the existence of high barriers and unstable intermediate states. H diffusion into the bulk is an endothermic process and inhibited by the initial rotation step, making it uncompetitive with surface processes of H.

At reduced $CeO_2(111)$, we find that O vacancies increases the electronic charges at adjacent surface O through the occurrence of $Ce^{3+}$. These excess charges reduce their capability of accepting more electrons. As a result, weaker O-H bonds would form after H adsorption, which significantly affects the reactions and diffusions of H. In particular, the H coupling process, which requires complete O-H bond breaking, benefits from the weak O-H bond. For $H_2O$ formation, on the other hand, such electronic effect is less significant at different reduced surfaces. Therefore, the H coupling pathway would be relatively favored at heavily reduced $CeO_2(111)$. The weak O-H interactions at reduced $CeO_2(111)$ also help the surface and bulk diffusion of H.

In general, our results can help to obtain a better picture of H-ceria interacting systems. Moreover, some quantitative rules that can help to judge the adsorption strength and pathway selectivity of H at oxide surfaces have been proposed. We believe that it can facilitate design of more effective catalysts in H-related reactions at ceria based and many other catalysts.

## Acknowledgements

This work was supported by the National Basic Research Program (2011CB808505), National Natural Science Foundation of China (21322307, 21421004), Open Project of State Key Laboratory of Chemical Engineering (SKL-ChE-12C02) and "Shu Guang" project of Shanghai Municipal Education Commission and Shanghai Education Development Foundation (13SG30). The authors also thank the computing time in the National Super Computing Center in Jinan.

## Notes

[a] *Key Laboratory for Advanced Materials and Centre for Computational Chemistry, East China University of Science and Technology, 130 Meilong Road, Shanghai 200237, P.R. China.*

[b] *Key Laboratory for Advanced Materials and Research Institute of Industrial Catalysis, East China University of Science and Technology, 130 Meilong Road, Shanghai 200237, P.R. China.*

[*] *Corresponding authors: xgong@ecust.edu.cn, gzhlu@ecust.edu.cn*

† Electronic Supplementary Information (ESI) available: Calculated route of H bulk diffusion, oxygen vacancy formation energies for $CeO_2(111)$ with one and three surface O vacancies, optimized structures of $CeO_2(111)$ with one and three O vacancies, corresponding structures of surface reactions of H, energy barrier values for surface reactions, surface diffusion and bulk diffusion of H, structures for surface and bulk diffusions of H, O-H bond energy. See DOI: 10.1039/b000000x/

## References

1 W. C. Chueh, C. Falter, M. Abbott, D. Scipio, P. Furler, S. M. Haile and A. Steinfeld, *Science*, 2010, **330**, 1797.
2 S. Abanades and G. Flamant, *Solar Energy*, 2006, **80**, 1611.
3 P. Furler, J. R. Scheffe and A. Steinfeld, *Energy Environ. Sci.*, 2012, **5**, 6098.
4 B. C. H. Steele and A. Heinzel, *Nature*, 2001, **414**, 345.
5 E. P. Murray, T. Tsai and S. A. Barnett, *Nature*, 1999, **400**, 649.
6 R. J. Gorte, H. Kim and J. M. Vohs, *J. Power Sources*, 2002, **106**, 10.
7 S. Mclntosh and R. J. Gorte, *Chem. Rev.*, 2004, **104**, 4845.
8 M. V. Martinez-Huerta, J. M. Coronado, M. Fernández-Garcia, A. Iglesias-Juez, G. Deo, J. L. G. Fierro and M. A. Bañares, *J. Catal.*, 2004, **225**, 240.
9 M. V. Martinez-Huerta, G. Deo, J. L. G. Fierro and M. A. Bañares, *J. Phys. Chem. C*, 2007, **111**, 18708.
10 M. V. Martinez-Huerta, G. Deo, J. L. G. Fierro and M. A. Bañares, *J. Phys. Chem. C*, 2008, **112**, 11441.

11 M. V. Ganduglia-Pirovano, C. Popa, J. Sauer, H. Abbott, A. Uhl, M. Baron, D. Stacchiola, O. Bondarchuk, S. Shaikhutdinov and H. J. Freund, *J. Am. Chem. Soc.*, 2010, **132**, 2345.
12 H. L. Abbott, A. Uhl, M. Baron, Y. Lei, R. J. Meyer, D. J. Stacchiola, O. Bondarchuk, S. Shaikhutdinov and H. J. Freund, *J. Catal.*, 2010, **272**, 82.
13 H. T. Chen, Y. M. Choi, M. L. Liu and M. C. Lin, *ChemPhysChem*, 2007, **8**, 849.
14 S. Bernal, J. J. Calvino, G. A. Cifredo, J. M. Gatica, J. A. Pérez-Omil and J. M. Pintado, *J. Chem. Soc. Faraday Trans.*, 1993, **89**, 3499.
15 J. L. G. Fierro, J. Soria, J. Sanz and J. M. Rojo, *J. Solid State Chem.*, 1987, **66**, 154.
16 J. L. G. Fierro, S. Mendioroz and A. M. Olivan, *J. Colloid Interf. Sci.*, 1985, **107**, 60.
17 L. A. Bruce, M. Hoang, A. E. Hughes and T. W. Turney, *Appl. Catal. A: Gen.*, 1996, **134**, 351.
18 K. Sohlberg, S. T. Pantelides and S. J. Pennycook, *J. Am. Chem. Soc.*, 2001, **123**, 6609.
19 D. M. Lyons, J. P. McGrath and M. A. Morris, *J. Phys. Chem. B*, 2003, **107**, 4607.
20 D. M. Lyons, K. M. Ryan and M. A. Morris, *J. Mater. Chem.*, 2002, **12**, 1207.
21 C. T. Campbell and C. H. F. Peden, *Science*, 2005, **309**, 713.
22 B. Chen, Y. Ma, L. Ding, L. Xu, Z. Wu, Q. Yuan and W. Huang, *J. Phys. Chem. C*, 2013, **117**, 5800.
23 G. Kresse and J. Furthmüller, *Comput. Mater. Sci.*, 1996, **6**, 15.
24 G. Kresse and J. Hafner, *Phys. Rev. B*, 1994, **49**, 14251.
25 P. E. Blöchl, *Phys. Rev. B*, 1994, **50**, 17953.
26 S. Fabris, G. Vicario, G. Balducci, S. D. De Gironcoli and S. Baroni, *J. Phys. Chem. B*, 2005, **109**, 22860.
27 M. Nolan, S. C. Parker and G. W. Watson, *Surf. Sci.*, 2005, **595**, 223.
28 M. Nolan, S. Grigoleit, D. C. Sayle, S. C. Parker and G. W. Watson, *Surf. Sci.*, 2005, **576**, 217.
29 E. A. Kummerle and G. Heger, *J. Solid State Chem.*, 1999, **147**, 485.
30 G. Mills and H. Jónsson, *Phys. Rev. Lett.*, 1994, **72**, 1124.
31 G. Mills, H. Jónsson and G. K. Schenter, *Surf. Sci.*, 1995, **324**, 305.
32 G. Henkelman and H. Jónsson, *J. Chem. Phys.*, 2000, **113**, 9978.
33 G. Henkelman, B. P. Uberuaga and H. Jónsson, *J. Chem. Phys.*, 2000, **113**, 9901.
34 M. V. Ganduglia-Pirovano, J. L. F. Da Silva and J. Sauer, *Phys. Rev. Lett.*, 2009, **102**, 026101.
35 H. Y. Li, H. F. Wang, X. Q. Gong, Y. L. Guo, Y. Guo, G. Z. Lu and P. Hu, *Phys. Rev. B*, 2009, **79**, 193401.
36 G. Vicario and G. Balducci, *J. Phys. Chem. B*, 2006, **110**, 19380.
37 G. Henkelman, A. Arnaldsson and H. Jónsson, *Comput. Mater. Sci.*, 2006, **36**, 354.
38 E. Sanville, S. D. Kenny, R. Smith and G. Henkelman, *J. Comp. Chem.*, 2007, **28**, 899.
39 W. Tang, E. Sanville and G. Henkelman, *J. Phys.: Condens. Matter*, 2009, **21**, 084204.